Ultrasensitive detection of protein translocated through toxin pores in droplet-interface bilayers

Audrey Fischer[a], Matthew A. Holden[b,1], Brad L. Pentelute[a], and R. John Collier[a,1]

[a]Department of Microbiology and Molecular Genetics, Harvard Medical School, 200 Longwood Avenue, Boston, MA; and [b]Department of Chemistry, University of Massachusetts, 710 North Pleasant Street, Amherst, MA

Contributed by R. John Collier, August 10, 2011 (sent for review June 15, 2011)

Many bacterial toxins form proteinaceous pores that facilitate the translocation of soluble effector proteins across cellular membranes. With anthrax toxin this process may be monitored in real time by electrophysiology, where fluctuations in ionic current through these pores inserted in model membranes are used to infer the translocation of individual protein molecules. However, detecting the minute quantities of translocated proteins has been a challenge. Here, we describe use of the droplet-interface bilayer system to follow the movement of proteins across a model membrane separating two submicroliter aqueous droplets. We report the capture and subsequent direct detection of as few as 100 protein molecules that have translocated through anthrax toxin pores. The droplet-interface bilayer system offers new avenues of approach to the study of protein translocation.

Many toxins produced by pathogenic bacteria (e.g., anthrax, diphtheria, botulinum toxins) have the ability to cross membranes and enzymatically modify substrates within the cytosolic compartment of mammalian cells (1). Most of these toxins are bipartite entities, consisting of a catalytic polypeptide and a transport polypeptide. The latter binds to cellular receptors and in some cases has the additional property of being able to form ion-conductive pores in model membranes, such as planar phospholipid bilayers and liposomes (2–4). For some toxins there is considerable evidence that these pores are functionally relevant to the transport of cognate catalytic moieties ("cargo" proteins) across cellular membranes (3). In anthrax toxin, for example, cargo molecules block current through the pores formed by the protective antigen (PA) moiety, and after an appropriate electrical potential or a proton gradient is applied, the current is restored to the pore's open-state level, suggesting translocation of the cargo (5–8). A number of control experiments support this interpretation (5, 7–9). Detecting and assaying cargo protein in the *trans* chamber, opposite to that to which the protein was added, has proven challenging, however, mainly because the quantities of the cargo believed to be translocated are so small. To date there is only one report of detection of a cargo protein translocated into the *trans* chamber of planar bilayer systems (10).

In the study reported here we used an alternative model membrane system for detecting translocated cargo proteins. Instead of a planar bilayer, we used the recently developed droplet-interface bilayer (DIB) (11–13). Briefly, aqueous droplets immersed in a hydrocarbon/phospholipid mixture spontaneously acquire lipid monolayer shells at the oil–water interface. When two such droplets are moved into contact with one another, a lipid bilayer membrane (DIB) forms at the interface. An electrode is embedded in each droplet, allowing electrophysiological monitoring of bilayer formation and pore activity, and each electrode is attached to a micromanipulator, allowing precise positioning of the droplets.

Several advantages are realized with the DIB system. The small volume of the droplets, typically ≤200 nanoliters, permits capture of translocated cargo molecules at concentrations orders of magnitude higher than in experiments with traditional planar bilayers (2, 5, 6, 8), where compartment size is typically approximately 1 mL. The size of the bilayer can be adjusted by positioning the droplets relative to one another with the micromanipulators, and the ratio of bilayer area to capture volume may thereby be maximized (12, 13). Because the capture droplet is surrounded by a lipid monolayer and submerged in hexadecane, loss of cargo due to nonspecific adsorption to container surfaces and loss of water due to evaporation are prevented. Most importantly, and unique to the DIB method, one can "unzip" the bilayer by using the micromanipulators to pull the electrodes apart, thereby separating the droplets (Fig. 1). Any translocated molecule then resides in a tiny, easy-to-handle, aqueous sphere, protected by the surrounding monolayer.

In the current study we used the DIB system to study protein translocation through the anthrax toxin pore (3, 8). Anthrax toxin belongs to the binary toxin family, a category in which enzymatic proteins interact noncovalently with a cognate pore-forming protein. In anthrax toxin, PA, (83 kDa), which has both receptor binding and pore-forming activities, serves as the transporter of two discrete enzymatic proteins: LF (Lethal Factor, 90 kDa), a metalloprotease that inactivates most members of the mitogen activated protein kinase kinase family, and Edema Factor (EF, 89 kDa), a Ca^{++}- and calmodulin-dependent adenylyl-cyclase, (3). After binding to a mammalian cell-surface receptor, PA is cleaved by furin, yielding an active 63-kDa fragment (PA_{63}) (14, 15). Receptor-bound PA_{63} self-associates to form heptameric (16) or octameric (17) oligomers (prepores), which are capable of binding LF and EF competitively and with high affinity ($K_d \sim 1$ nM). Complexes of prepore and the enzymatic moieties are then endocytosed. Upon exposure to acidic conditions within the endosome, the prepore undergoes a conformational transition that allows it to insert into the membrane and translocate bound LF and/or EF to the cytosolic compartment (18). LF and EF may bind to PA_{63} oligomers and undergo translocation independently of each other.

Here we describe a two-step protocol to detect cargo molecules transported across a DIB via heptameric PA_{63} pores (Fig. 1). For cargo protein we used the N-terminal domain of LF (LF_N), which has been extensively studied as a model translocation substrate in planar bilayers, or a hexahistidine-tagged form of this domain (hLF_N) (5, 19, 20). In step 1 a DIB is formed between a droplet (the "reservoir" droplet), containing PA_{63} plus cargo protein, and another (the "capture" droplet), consisting of an agarose hydrogel sphere. One or more cycles of translocation of cargo are induced by voltage and monitored by electrophysiology. The capture droplet is then separated from the reservoir droplet. In step 2 the reservoir droplet is discarded, a small quantity of PA_{63} prepore is added to the capture droplet, and this droplet is joined with a fresh protein-free droplet, termed the "detection"

Author contributions: A.F., M.A.H., and B.L.P. designed research; A.F. performed research; M.A.H. contributed new reagents/analytic tools; A.F., M.A.H., B.L.P., and R.J.C. analyzed data; and A.F., M.A.H., B.L.P., and R.J.C. wrote the paper.

Conflict of interest statement: R.J.C. holds equity in PharmAthene, Inc.

[1]To whom correspondence may be addressed. E-mail: jcollier@hms.harvard.edu or mholden@chem.umass.edu.

This article contains supporting information online at www.pnas.org/lookup/suppl/doi:10.1073/pnas.1113074108/-/DCSupplemental.

droplet, to generate a second DIB. The added PA_{63} forms pores in this DIB that serve as an electropysiological detector for captured cargo molecules. This approach has enabled us to detect as few as 100 cargo molecules in the capture droplet.

Results

PA Pore Activity in DIB Membranes. First we coated two electrodes with 2% agarose in pH 5.5 bilayer buffer and then immersed the tips of the electrodes in 0.25 mL hexadecane containing 5 mM 1,2-diphytanoyl-*sn*-glycero-3-phosphocholine. To form the reservoir droplet we attached to one of the agarose-coated electrodes a 200 nL droplet containing PA_{63} heptamer alone or heptamer with an equimolar amount of the cargo protein. The capture droplet consisted simply of the agarose bead surrounding the reference electrode. The reservoir and capture compartments were held apart in the lipid/oil solution for 30 min before being moved into contact with each other. After bilayer formation, as detected by capacitance changes, the position of the capture electrode was adjusted until the bilayer diameter was approximately 200 μm (Fig. S1), and the bilayer was held for approximately 5 min at a membrane potential ($\Delta\Psi$) of +20 mV, where $\Delta\Psi = \Psi_{reservoir} - \Psi_{capture}$ ($\Psi_{capture} \equiv 0$ mV).

By measuring current we were routinely able to monitor 1,000 to 2,000 PA_{63} pores in an individual DIB, while retaining bilayer stability for ≥1 hr. The properties of the PA pores in DIBs were nearly identical to those of pores in planar bilayers under the same conditions, as assessed by various measures (7). Thus, WT PA_{63} pores showed single-pore (single-channel) conductance values of approximately 44 ± 2 pS in 100 mM KCl, were primarily open at positive applied potentials, and became inactive over time at negative potentials (Figs. S2*A* and S3*A*). Mutated forms of PA_{63} had similar properties in the two systems; for example, presence of the F427D mutation in a single subunit of the PA_{63} heptamer caused a 2.2-fold increase in single-pore conductance in the DIB system, identical to that seen in planar bilayers (Fig. S2*B*) (21).

Blocking of PA Pores by Cargo in DIB Membranes. After verifying there was no significant difference in the properties of PA_{63} pores in planar bilayers from those in DIBs, we conducted further control experiments in the presence of cargo proteins. At an applied potential of +20 mV, an equimolar amount of LF_N and PA in the reservoir droplet caused approximately 43% blockage of current (i.e., current was completely blocked in approximately 43% of the pores), and this value remained relatively stable over time (Table S1). The total number of pores, blocked plus not blocked, was determined from the current measured after reversing the polarity of the applied potential. This reversal caused the N terminus of the cargo protein to withdraw from blocked pores, allowing free passage of ions. Under the same conditions hLF_N caused approximately 83% blockage, consistent with results in planar bilayers showing that a tract of basic amino acids appended to the N terminus of LF_N increased affinity for the pore (5, 19).

Translocation of Cargo Across DIB Membranes. After WT PA_{63} pores were blocked by hLF_N at $\Delta\Psi = +20$ mV, raising the voltage to a value between +50 mV and +80 mV caused pore current to increase (i.e., caused pores to be unblocked) (8). Current restoration, reflecting cargo translocation, was essentially complete within 10 s after raising $\Delta\Psi$ to +60 mV or higher but was slower at +50 mV (Fig. 2*A*). The minimal number of cargo molecules translocated was estimated from the number of pores that became unblocked, a value calculated by dividing the current change by $\Delta\Psi$ and the single-pore conductance (44 pS). The current change of the representative trace shown in Fig. 2*B* is approximately 4.8 nA, corresponding to about 1,300 molecules of hLF_N translocated, based on the assumption that each pore is completely blocked by a single hLF_N molecule. Although each heptameric pore is capable of binding up to three molecules of cargo simultaneously (3), we routinely added the same number of cargo molecules as heptamers, thereby dictating the average occupancy. In some experiments, after the initial translocation event, we cycled the applied voltage one or more times to increase the pool of translocated cargo. Each cycle involved reducing $\Delta\Psi$ to +20 mV, then allowing 10 min for the pores to become reblocked by cargo from the aqueous solution, and finally elevating $\Delta\Psi$. By such repetition we were able to translocate an estimated several thousand molecules of cargo into the capture droplet.

Detection of Translocated Cargo. To test for the presence of cargo protein in the capture droplet, we first separated this droplet from the reservoir droplet, while monitoring capacitance to ensure that the barrier between the two droplets was not compromised during the separation (Fig. S1*C*). The reservoir droplet

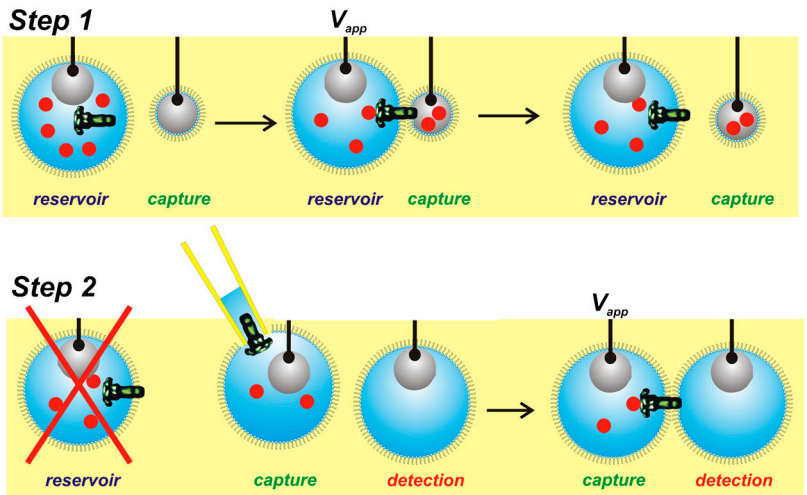

Fig. 1. Protocol for study of anthrax toxin translocation in the DIB system. Step 1: Two electrodes coated in 2% agarose (gray) are suspended in lipid-hexadecane solution (yellow), and a 200-nL droplet containing PA_{63} (black) and LF_N (red) in bilayer buffer is added to one of the electrodes to form the reservoir droplet. After contact of the reservoir and capture droplets, a bilayer is formed, and PA_{63} pores insert. Following translocation of cargo, stimulated by elevated membrane potential, the droplets are separated. Step 2: The reservoir droplet is removed and discarded, and a detection droplet is formed by adding a 200-nL droplet of bilayer buffer to a new agarose-coated electrode. The capture droplet is supplemented with 200 nL of diluted PA_{63}, and a DIB is formed with the detection droplet. Upon PA_{63}-membrane incorporation, blockage of the pores by cargo from the capture droplet is monitored at the single-pore level.

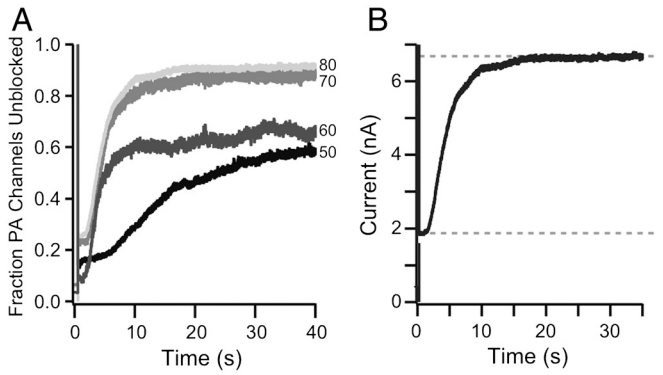

Fig. 2. Voltage driven translocation of hLF_N across DIB membranes. (*A*) Translocation through WT PA_{63} pores was initiated at $t = 0$ s by increasing $\Delta\Psi$ from +20 mV to higher values, as indicated. Heptameric PA_{63} and hLF_N were present at equimolar concentrations. At $\Delta\Psi = +50$ mV, $t_{1/2} \sim 10$ s, 59% translocation; at $\Delta\Psi = +60$ mV $t_{1/2} \sim 4$ s, 68% translocation; at $\Delta\Psi = +70$ mV, $t_{1/2} \sim 4$ s, 74% translocation; and at $\Delta\Psi = +80$ mV $t_{1/2} \sim 3$ s, 83% translocation. (*B*) Representative current trace at +80 mV, showing a current change of approximately 4.8 nA, corresponding to approximately 1,300 translocated hLF_N.

was then discarded, and a 200-nL droplet containing 1.5 nM PA_{63} heptamers in bilayer buffer was fused into the capture bead. After appropriate incubation to ensure that the phospholipid monolayer had been restored, a new DIB was formed between the PA_{63}-supplemented capture droplet and a new protein-free droplet, the detection droplet. Finally, a potential of +80 mV, +50 mV, or +20 mV was applied across the DIB, and single-molecule pore activity was monitored, with the capture droplet now representing the *cis* compartment (Fig. 3 and Fig. S4).

In trials in which an estimated 5,000 molecules of hLF_N had been translocated into the capture droplet in step 1, we observed a high frequency of pore-blocking events in step 2 at all three values of $\Delta\Psi$ (Fig. 3 *B* and *Eb*). A similar frequency of blocking events was seen in traces recorded with a control droplet supplemented with 5,000 molecules of hLF_N and 1.5 nM PA_{63} WT (Fig. 3 *A* and *Ea*). The level of pore-blocking activity was well above background when as little as 100 molecules of this cargo protein were added into a control capture droplet (Fig. 3*Eb*) or when an estimated 100 molecules were translocated into this droplet from the reservoir droplet (Fig. 3 *C* and *Ed*).

Controls demonstrated that cargo molecules detected in the capture droplet following step 1 had in fact entered that droplet via PA_{63} pores in the DIB. No pore-blocking events were detected in step 2 when hLF_N was present in the reservoir droplet lacking PA_{63} (Fig. 3 *D* and *Ef*), which showed that cargo did not passively cross the DIB or diffuse from the reservoir droplet to the capture droplet via the oil phase. Also, pore blockage in step 2 was virtually at background levels when, in step 1, we used a translocation-deficient form of PA_{63} (F427H) (7, 22) with hLF_N (Fig. 3*Eg*) or when we held $\Delta\Psi$ at +20 mV (Fig. 3*E* and Fig. S3).

Detection of translocated cargo in step 2 was sensitive to mutations known to affect LF_N binding. Pore occlusion was essentially nil when WT PA_{63} added to the capture droplet in step 2 was replaced by either the F427H single mutant (21) or the R178A/K214E double mutant (23) (Fig. 4). The F427 residues of the oligomeric pore form a structure called the Phe clamp (7), which interacts with the unstructured extreme N terminus of LF_N (23), and the F427H mutation blocks this interaction, perhaps by electrostatic repulsion. R178 is a key residue in a site within PA_{63} prepore (the α site) that binds the α1 and β1 structures of LF_N (24), and K214 forms part of the domain 1′ surface of PA_{63} that recognizes the globular part of LF_N (24). The R178A/K214E double mutation drastically reduces binding of LF_N and occlusion of the pore (23, 24).

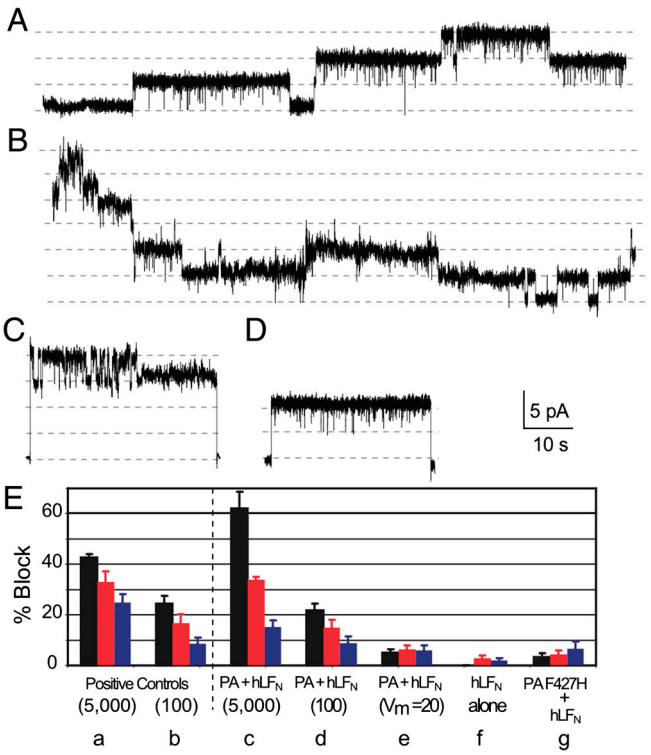

Fig. 3. Detection of hLF_N translocated into the capture droplet (step 2). hLF_N was translocated into the capture hydrogel via WT PA_{63} pores. (*A–D*) Representative current traces of PA_{63} pore activity in the DIB formed between the capture and detection droplets at $\Delta\Psi = +80$ mV. The dotted lines in *A–D* represent transitions between the blocked and open states of PA pores. For current traces *C* and *D* the voltage was briefly held at 0 mV before and after the +80 mV pulse in order to visualize the baseline signal. (A) Control in which a known amount of 5,000 hLF_N molecules were directly introduced into a blank capture droplet in step 2. (*B*) An estimated 5,000 hLF_N molecules were translocated to the capture droplet. (*C*) An estimated approximately 100 hLF_N molecules were translocated into the capture droplet; only one of the four PA_{63} pores transitioned to the closed state. (*D*) PA_{63} was omitted from the reservoir droplet in step 1. (*E*) Average % block of WT PA_{63} pore activity under various conditions, at applied $\Delta\Psi$ values of +80 mV (black), +50 mV (red), or +20 mV (blue), across the capture:detection DIB. (*a* and *b*) Controls in which 5,000 (*a*, $n = 3$) or 100 (*b*, $n = 5$) hLF_N molecules were directly added to a blank capture droplet. (*c* and *d*) An estimated 5,000 (*c* $n = 4$) or 100 (*b*, $n = 3$) molecules of hLF_N were translocated into the capture droplet. (*e*) $\Delta\Psi$ was maintained at +20 mV in step 1 ($n = 3$). (*f*) PA_{63} was omitted from the reservoir droplet in step 1. (*g*) PA_{63}-F427H replaced WT PA_{63} in step 1 ($n = 3$). Average number of opening events analyzed per data point was 689.

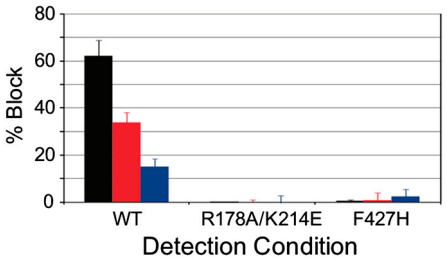

Fig. 4. Requirement for WT PA_{63} pores for detection of translocated hLF_N in step 2. In step 1, 5,000 molecules of hLF_N were translocated into the capture droplet via WT PA_{63} pores. The capture and reservoir droplets were then separated, and 200 nL 1.5 nM WT or mutant PA_{63} was added to the capture hydrogel. Representative % blockage activities of WT ($n = 4$), R178A/K214E ($n = 3$), and F427H ($n = 3$) pores are shown at +80 mV (black), +50 mV (red), and +20 mV (blue) (average number of opening events analyzed per data point = 566).

Discussion

While results of electrophysiological studies leave little doubt that one can reproduce anthrax toxin translocation across the endosomal membrane in classical phospholipid bilayer systems, data demonstrating the actual physical transfer of cargo protein from the *cis* to the *trans* compartment of such systems have been lacking. The DIB system offered the possibility of demonstrating such transfer because of two potentially important advantages over the planar bilayer system. First, because the area of the bilayer and the number of pores are more or less unchanged from the planar bilayer system, the approximately 5,000-fold lower chamber volume of the DIB translates into a corresponding increase in cargo concentration, facilitating detection. Second, the DIB system offered the possibility of "unzipping" the bilayer, and thus physically separating the *trans* compartment from the *cis* following translocation, Hence, the *trans* compartment (capture droplet) could be isolated as a discrete unit and analyzed for the presence of translocated cargo protein.

For detection of cargo translocated into in the capture droplet we have used blockage of PA_{63} pore conductance as a signal. While highly sensitive and readily available, this approach necessitated forming a new set of pores and a new bilayer. We observed no evidence of pore retention in the capture droplet after it was separated from the reservoir droplet and presume that the pores in the original DIB remained associated with the latter. As a source of new pores PA_{63} was readily introduced into the capture droplet with a micropipet. The phospholipid monolayer surrounding the droplet was necessarily perturbed by this operation, but it reformed by accretion of phospholipid from the hexadecane solution. A bilayer could then be generated with a blank detection droplet, and inserted PA_{63} pores could serve as a sensitive biosensor of the translocated cargo. This detection system proved to be robust and allowed reproducible detection of cargo, down to approximately 100 molecules (approximately 800 aM) (Fig. 3 *Eb* and *Ed*).

For the purpose of this initial study in the DIB system, we used membrane potential as the driving force of translocation and LF_N as model, single-domain cargo. Membrane potential could be varied simply by voltage clamping, whereas generating and maintaining a transmembrane proton gradient presented challenges, a limitation of the DIB system. LF_N is known to serve as an efficient translocation substrate in planar bilayers, had been extensively characterized (5–9, 19–21, 25–28), and was the obvious cargo protein of choice. The enhanced pore-blocking activity resulting from appending an N-terminal hexahistidine tag led us to use the hLF_N derivative in most experiments.

The fact that WT PA_{63} served effectively to detect cargo in the capture droplet, whereas either of two binding-deficient forms of PA did not, suggests that the protein refolded to its native configuration after translocation (Fig. 4). At least for this simple, single-domain cargo protein, the toxin itself may therefore contain all of the molecular machinery needed for translocation across the bilayer and refolding. Our findings do not, however, preclude a requirement for cellular factors to aid translocation across the endosomal membrane and refolding in vivo, particularly of complex, multidomain cargo proteins. Recent reports with lethal toxin and variants suggest that cellular proteins such as Hsp90 (29), CypA (29), and COP1 coatomer complex (30) are important in mediating cytotoxicity in cellular systems. The application of DIBs to study anthrax toxin protein translocation may aid investigations to probe the possibility that such factors assist transport through PA pores. With the DIB system, the ultralow volume droplets may allow this process to be probed while consuming small amounts of precious chaperonin material.

It should be possible to adapt the DIB technology to enable investigators to detect translocated cargo proteins by other methods besides pore blockage (e.g., fluorescence). Also, modifications of the DIB technology may allow some of its inherent limitations to be circumvented (e.g., the inability to perfuse individual droplets to remove reagents, replace buffers, and the like). Such modifications would facilitate application of the DIB technology to other intracellularly acting toxins and to protein transport systems unrelated to pathogenesis.

Materials and Methods

Materials. Biochemical reagents were purchased from Fisher Scientific unless indicated otherwise. Nα-(3-maleimidylpropionyl)-biocytin was obtained from Invitrogen—Molecular Probes, and UltraLink immobilized monomeric avidin was obtained from Pierce.

Expression and Purification of Proteins. Recombinant WT PA and PA mutants were grown in ECPM1 (31) medium and overexpressed in the periplasm of *Escherichia coli* BL21 (DE3) before purification by anion-exchange chromatography (32). The heteroheptameric PA_{63} $[F427D]_1[WT]_6$ mutant PA protein contained two mutations, K563C and F427D, and was generated as previously described (9). WT PA_{63} and homoheptameric PA_{63} R178A/K214E prepore were formed by limited trypsin digestion and purified by anion-exchange chromatography, as previously described (23, 33, 34). The N-terminal domain of LF (LF_N) WT and mutants were prepared as previously described (5).

Electrophysiology. DIBs were formed and analyzed using a custom imaging/micromanipulation platform (12) with a Nikon SMZ 800 Zoom stereo microscope and Axopatch 200B amplifier (Molecular Devices) using pClamp 10.2 acquisition software (Molecular Devices). Records were acquired at a sampling frequency 2 kHz and filtered online to 0.1 kHz with a Gaussian filter. All experiments were conducted at 22 ± 2 °C. A sterile Eppendorf tube cap served as the bilayer chamber and was filled with 0.25 mL of 5 mM 1,2-diphytanoyl-*sn*-glycero-3-phosphocholine in hexadecane. After treatment with sodium hypochlorite solution for approximately 15 min, the Ag/AgCl electrode tips were coated to form a bead in 2% low melt agarose pH 5.5 bilayer buffer. The bilayer buffer contained 100 mM KCl, 1 mM ethylenediaminetetraacetic acid, and 10 mM each of sodium oxalate, potassium phosphate, and 2-(N-morpholino)ethanesulfonic acid. The pH of the bilayer buffer was adjusted to a final value of 5.5 with KOH. A 200 nL drop of bilayer buffer, supplemented with PA_{63} heptamer alone or PA_{63} heptamer with equimolar LF_N (unless otherwise stated), was added to the tip of the stimulatory electrode that contained an agarose bead to form the aqueous reservoir droplet. The capture hydrogel comprised of the 2% agarose, pH 5.5 bilayer buffer bead around the reference electrode tip. The reservoir and capture compartments were submerged in the lipid/oil solution for 30 min before being moved to touch each other as visualized with the stereo microscope. Upon bilayer nucleation, the capture electrode was moved away from the reservoir droplet until the bilayer diameter was approximately 200 μm, as monitored by triangle wave pulse shown in Fig. S1. The pipette offset was adjusted to zero; then the bilayer was allowed to stabilize for approximately 5 min at a holding potential of +20 mV. The membrane potential ($\Delta\Psi$) was defined as $\Delta\Psi = \Psi_{cargo} - \Psi_{capture}$, where $\Psi_{capture} \equiv 0$ mV.

PA_{63} Pore Formation, LF_N Conductance Block, and Voltage-Driven Translocation. Once a membrane was formed in the DIB system, PA_{63} ion conductance was monitored and found to increase over time. In order to monitor LF_N translocation, PA_{63} and LF_N were preincubated together at pH 8.5 before dilution into pH 5.5 bilayer buffer and then added to the reservoir electrode. LF_N block was induced for 5 min at +20 mV prior to voltage-dependent translocation, which was initiated by $\Delta\Psi = +50$ mV.

Detection of Translocated LF_N. Aqueous and hydrogel droplets were separated after LF_N translocation. The triangle wave pulse was used to monitor droplet separation in order to detect any capacitive spikes that would indicate bilayer fusion rather than clean separation. Once droplet separation was achieved, the reservoir droplet was moved as far as possible from the capture (Fig. 1). The reservoir electrode was removed from solution and treated with sodium hypochlorite solution for 5 min, and the tip was coated with a fresh agarose bead. The electrode was then submerged back into the oil/lipid mixture and a 200-nL droplet of bilayer buffer was added to form the detection droplet (Fig. 1). A 200-nL sample of 1.5-nM PA_{63} heptamer in bilayer buffer was added to the capture hydrogel bead. The electrode inputs were switched such that the membrane potential ($\Delta\Psi$) was defined as $\Delta\Psi = \Psi_{capture} - \Psi_{detection}$, where $\Psi_{detection} \equiv 0$ mV. The capture and detection droplets were held submerged in the lipid/oil solution separately for at least 30 min or until the surface tension of both droplets was relieved. A DIB was formed between the two aqueous droplets. Within 10 min of bilayer formation a single

PA_{63} pore inserted into the membrane. For most experiments a single-pore was monitored over the lifetime of the bilayer; however, some experiments had up to six clearly distinguishable pores insert in the membrane after 1 hr of recording. The bilayer was maintained at +20 mV for up to 10 min following onset of PA_{63} pore activity and the voltage was increased to +50 mV and +80 mV for periods of 60 s. The presence of LF_N in the detection droplet resulted in brief PA_{63} pore closing events of 100 ms at +20 mV; longer closing events were evident at increased positive membrane potentials.

Single-Pore Data Analysis. Single-pore analysis was performed on 60 s recordings using Clampfit, pClamp 10.2 (Molecular Devices). Single-pore ion conductance for PA_{63} was calculated from Gaussian fits to current amplitude histograms using Igor (Wavemetrics). The total number of opening events (N) analyzed was 99,679. The percent block of PA_{63} pores by LF_N was calculated as the fraction of time that the PA_{63} pore resided within the open state vs. the closed state for each recording; under positive membrane potentials PA_{63} does not regularly transition to the closed state on the time scale of the voltage pulses recorded (Fig. S2). Percent block was represented individually for each applied membrane potential as LF_N block of PA_{63} pores increased correspondingly with positive applied membrane potential.

Macroscopic Pore Data Analysis. The voltage-dependent block of PA_{63} s by LF_N was calculated from measurements of the fraction of time that the PA_{63} pores resided within the open state as a function of voltage. The total current due to unoccluded PA_{63} pore activity was calculated from voltage pulses to −50 mV—the applied membrane potential at which LF_N block was alleviated—immediately following each translocation event. The number of PA_{63} pores in the bilayer was determined from the total current divided by the applied voltage and γ. Macroscopic ion conductance block of PA_{63} by LF_N was determined from total instantaneous current at +50 mV divided by the unoccluded PA_{63} current at −50 mV. The rate of LF_N translocation through PA pore was determined as the time to alleviate half of ion conductance block ($t_{1/2}$). The minimum number of translocated cargo molecules was determined from the number of PA_{63} pores that became unoccluded during translocation. For this calculation, we assumed that one PA heptamer translocated a single cargo molecule during each translocation event. Statistical values represent means ± SEM; $n \geq 3$ for all experiments performed.

ACKNOWLEDGMENTS. We thank L. Perry and R. Ross at the Biomolecular Production Core of New England Regional Center of Excellence for helping with bacterial protein growth and expression of proteins used in this study [National Institutes of Health (NIH) Grant AI057159]. This work was supported by NIH Grant AI022021 (R.J.C.) and University of Amherst Department of Chemistry laboratory start-up grant (M.A.H.). We also thank Andrew J. McCluskey for technical and experimental assistance.

1. Alouf JE, Popoff MR (2006) *The Comprehensive Sourcebook of Bacterial Protein Toxins* (Elsevier, Amsterdam, Boston), 3rd ed, p xxiii, 1047.
2. Blaustein RO, Koehler TM, Collier RJ, Finkelstein A (1989) Anthrax toxin: Channel-forming activity of protective antigen in planar phospholipid bilayers. *Proc Natl Acad Sci USA* 86:2209–2213.
3. Young JA, Collier RJ (2007) Anthrax toxin: Receptor binding, internalization, pore formation, and translocation. *Annu Rev Biochem* 76:243–265.
4. Sun J, Vernier G, Wigelsworth DJ, Collier RJ (2007) Insertion of anthrax protective antigen into liposomal membranes: Effects of a receptor. *J Biol Chem* 282:1059–1065.
5. Zhang S, Finkelstein A, Collier RJ (2004) Evidence that translocation of anthrax toxin's lethal factor is initiated by entry of its N terminus into the protective antigen channel. *Proc Natl Acad Sci USA* 101:16756–16761.
6. Zhang S, Udho E, Wu Z, Collier RJ, Finkelstein A (2004) Protein translocation through anthrax toxin channels formed in planar lipid bilayers. *Biophys J* 87:3842–3849.
7. Krantz BA, et al. (2005) A phenylalanine clamp catalyzes protein translocation through the anthrax toxin pore. *Science* 309:777–781.
8. Krantz BA, Finkelstein A, Collier RJ (2006) Protein translocation through the anthrax toxin transmembrane pore is driven by a proton gradient. *J Mol Biol* 355:968–979.
9. Janowiak BE, Finkelstein A, Collier RJ (2009) An approach to characterizing single-subunit mutations in multimeric prepores and pores of anthrax protective antigen. *Protein Sci* 18:348–358.
10. Koriazova LK, Montal M (2003) Translocation of botulinum neurotoxin light chain protease through the heavy chain channel. *Nat Struct Biol* 10:13–18.
11. Funakoshi K, Suzuki H, Takeuchi S (2006) Lipid bilayer formation by contacting monolayers in a microfluidic device for membrane protein analysis. *Anal Chem* 78:8169–8174.
12. Holden MA, Needham D, Bayley H (2007) Functional bionetworks from nanoliter water droplets. *J Am Chem Soc* 129:8650–8655.
13. Hwang WL, Holden MA, White S, Bayley H (2007) Electrical behavior of droplet interface bilayer networks: Experimental analysis and modeling. *J Am Chem Soc* 129:11854–11864.
14. Molloy SS, Bresnahan PA, Leppla SH, Klimpel KR, Thomas G (1992) Human furin is a calcium-dependent serine endoprotease that recognizes the sequence Arg-X-X-Arg and efficiently cleaves anthrax toxin protective antigen. *J Biol Chem* 267:16396–16402.
15. Klimpel KR, Molloy SS, Thomas G, Leppla SH (1992) Anthrax toxin protective antigen is activated by a cell surface protease with the sequence specificity and catalytic properties of furin. *Proc Natl Acad Sci USA* 89:10277–10281.
16. Milne JC, Furlong D, Hanna PC, Wall JS, Collier RJ (1994) Anthrax protective antigen forms oligomers during intoxication of mammalian cells. *J Biol Chem* 269:20607–20612.
17. Kintzer AF, et al. (2009) The protective antigen component of anthrax toxin forms functional octameric complexes. *J Mol Biol* 392:614–629.
18. Abrami L, Lindsay M, Parton RG, Leppla SH, van der Goot FG (2004) Membrane insertion of anthrax protective antigen and cytoplasmic delivery of lethal factor occur at different stages of the endocytic pathway. *J Cell Biol* 166:645–651.
19. Pentelute BL, Barker AP, Janowiak BE, Kent SB, Collier RJ (2010) A semisynthesis platform for investigating structure-function relationships in the N-terminal domain of the anthrax Lethal Factor. *ACS Chem Biol* 5:359–364.
20. Basilio D, Kienker PK, Briggs SW, Finkelstein A (2011) A kinetic analysis of protein transport through the anthrax toxin channel. *J Gen Physiol* 137:521–531.
21. Janowiak BE, Fischer A, Collier RJ (2010) Effects of introducing a single charged residue into the phenylalanine clamp of multimeric anthrax protective antigen. *J Biol Chem* 285:8130–8137.
22. Sun J, Lang AE, Aktories K, Collier RJ (2008) Phenylalanine-427 of anthrax protective antigen functions in both pore formation and protein translocation. *Proc Natl Acad Sci USA* 105:4346–4351.
23. Jennings-Antipov LD, Song L, Collier RJ (2011) Interactions of anthrax lethal factor with protective antigen defined by site-directed spin labeling. *Proc Natl Acad Sci USA* 108:1868–1873.
24. Feld GK, et al. (2010) Structural basis for the unfolding of anthrax lethal factor by protective antigen oligomers. *Nat Struct Mol Biol* 17:1383–1390.
25. Thoren KL, Worden EJ, Yassif JM, Krantz BA (2009) Lethal factor unfolding is the most force-dependent step of anthrax toxin translocation. *Proc Natl Acad Sci USA* 106:21555–21560.
26. Kintzer AF, et al. (2010) Role of the protective antigen octamer in the molecular mechanism of anthrax lethal toxin stabilization in plasma. *J Mol Biol* 399:741–758.
27. Pentelute BL, Sharma O, Collier RJ (2011) Chemical dissection of protein translocation through the anthrax toxin pore. *Angew Chem Int Ed Engl* 50:2294–2296.
28. Brown MJ, Thoren KL, Krantz BA (2011) Charge requirements for proton gradient-driven translocation of anthrax toxin. *J Biol Chem*, 286 pp:89–99.
29. Dmochewitz L, et al. (2011) Role of CypA and Hsp90 in membrane translocation mediated by anthrax protective antigen. *Cell Microbiol* 13:359–373.
30. Tamayo AG, Bharti A, Trujillo C, Harrison R, Murphy JR (2008) COPI coatomer complex proteins facilitate the translocation of anthrax lethal factor across vesicular membranes in vitro. *Proc Natl Acad Sci USA* 105:5254–5259.
31. Bernard A, Payton M (2001) Fermentation and growth of *Escherichia coli* for optimal protein production. *Curr Protoc Protein Sci* Chapter 5: Unit5 3.
32. Miller CJ, Elliott JL, Collier RJ (1999) Anthrax protective antigen: prepore-to-pore conversion. *Biochemistry* 38:10432–10441.
33. Wang J, Vernier G, Fischer A, Collier RJ (2009) Functions of phenylalanine residues within the beta-barrel stem of the anthrax toxin pore. *PLoS One* 4:e6280.
34. Wigelsworth DJ, et al. (2004) Binding stoichiometry and kinetics of the interaction of a human anthrax toxin receptor, CMG2, with protective antigen. *J Biol Chem* 279:23349–23356.